2025 IEEE/RSJ International Conference on Intelligent Robots and Systems (IROS 2025)
October 19-25, 2025. Hangzhou, China

2025 IEEE/RSJ International Conference on Intelligent Robots and Systems (IROS) | 979-8-3315-4393-8/25/$31.00 ©2025 IEEE | DOI: 10.1109/IROS60139.2025.11246085

Physics-Informed Residual Network for Magnetic Dipole Model Correction and High-Accuracy Localization

Miaozhang Shen, *Student Member, IEEE*, Shuxiang Guo, *Fellow, IEEE*, Chunying Li, *Member, IEEE* and Zixu Wang, *Member, IEEE*

***Abstract*— The magnetic dipole model exhibits significant deviations from real-world sensor data due to neglected material nonlinearities and environmental interference. This paper proposed a Physics-Informed Residual Network (PIRNet) that adaptively corrected simulated magnetic field data by integrating dipole theory with deep residual learning. The network took a 5×5 triaxial magnetic matrix as input and employed a dual-branch architecture: a convolutional residual branch extracted local sensor-level distortion features, while a physics-encoding branch models systematic position and orientation-related deviations. A gated fusion mechanism dynamically combined these features, with a divergence-free constraint ($\nabla \cdot \mathbf{B} = 0$) incorporated as a regularization term. The corrected data was processed through Levenberg-Marquardt (LM) optimization for pose estimation, with subsequent hybrid lookup table compensation combining distance-weighted trilinear interpolation for spatial coordinates and spherical linear interpolation (Slerp) for orientation vectors. Experimental results showed that the positioning error was reduced from 2.1 mm to 1.15 mm, the orientation error was reduced from 3.23° to 1.01°, and the average speed of magnet positioning reached 44.7 ms per frame. This approach provides a high-precision, low-cost sim-to-real transfer solution for magnetic navigation robots.**

I. Introduction

Magnet localization is essential in various applications, including robotic systems, medical devices [1]–[3], and industrial automation [4]–[6]. Precise positioning of magnets is crucial for tasks such as magnetic actuation, autonomous navigation, and targeted drug delivery [7]–[9]. However, achieving high accuracy in single-magnet localization remains challenging due to discrepancies between the magnetic fields predicted by analytical models and those generated by real magnets. Traditional models, such as the dipole model [10], offer simplicity but lack the precision necessary to capture the complex geometrical and magnetization properties of actual magnets. While more detailed analytical models can improve accuracy, they often incur significantly increased computational complexity, rendering them less practical for real-time applications [11], [12].

Research in this field can be traced back to Schlageter et al. [13], who validated the effectiveness of the dipole model for far-field localization using a 4×4 Hall sensor array, although they did not account for model deviations induced by near-field geometric effects. Their work was the first to demonstrate that the magnetic field estimation error of the dipole model can reach up to 30% at extremely close distances ($r \leq 8r_m$, where r_m is the magnet radius). Subsequent theoretical breakthroughs have focused on optimizing three-dimensional magnetic field representation models. For instance, Masiero et al. [10] developed an analytical model for programmable magnetization in cylindrical magnets that improved gradient computation accuracy by 21% within a 60 mm working distance; however, the numerical integration approach used increased computational complexity by 47%.

In terms of iterative magnetic field inversion algorithms, the literature reveals two evolving paths: model-based and data-driven approaches. In traditional optimization methods, the Levenberg-Marquardt (LM) algorithm is widely used for magnet localization due to its efficiency and robustness. However, LM can become trapped in local minima, leading to suboptimal estimates of magnet positions and orientations. To address this issue, some studies have employed PSO algorithms, which explore the solution space more thoroughly to achieve improved accuracy. Despite these advantages, PSO algorithms often suffer from high computational costs and longer processing times. Zhang et al. [12] developed a hybrid algorithm that combines global search via PSO with local iteration using LM for capsule endoscope localization, achieving an average accuracy of 1.8 mm (for $z \in [60\,\text{mm}, 140\,\text{mm}]$), but they did not resolve the modeling bias in magnet moment estimation caused by sensor nonlinear responses.

Data-driven deep learning approaches have opened new avenues to overcome the limitations of traditional models [14]. Su et al. [11] developed the AMagPoseNet framework, which employs dual-domain few-shot learning to achieve real-time six-degree-of-freedom estimation (with a localization error of 1.15 mm and a per-frame processing time of 44.7 ms), thereby reducing the requirement for real data to only 4.9%. However, its end-to-end architecture lacks explicit physical constraints, resulting in a 38% increase in the probability of pose divergence under extremely near-

*Research supported by the Shenzhen "Medical Engineering Integration" Special Support Program Project under Grant F-2024-Z99-502365, Shenzhen, China; in part by the High level of special funds from Southern University of Science and Technology under Grant G03034K003, Shenzhen, China.

Corresponding authors: Shuxiang Guo.

Miaozhang Shen is with Advanced Institute for Ocean Research, Southern University of Science and Technology, Shenzhen, China. (e-mails:shenmz2024@mail.sustech.edu.cn).

Shuxiang Guo is with the Department of Electronic and Electrical Engineering, Southern University of Science and Technology, Shenzhen, China, also with the Aerospace Center Hospital, School of Life Science and the Key Laboratory of Convergence Medical Engineering System and Healthcare Technology, Ministry of Industry and Information Technology, Beijing Institute of Technology, Beijing, China (guo.shuxiang@sustech.edu.cn).

Chunying Li and Zixu Wang are with Department of Electronic and Electrical Engineering, Southern University of Technology and Science, Shenzhen, China (e-mails: licy@sustech.edu.cn; wangzx3@sustech.edu.cn).

field conditions ($z < 30$ mm) due to magnetic field saturation. Other studies have attempted to fuse model-based and data-driven approaches. For example, Guo et al. [15] proposed a ResNet-LM hybrid architecture that uses residual learning to suppress sensor noise (yielding an SNR improvement of 15.7 dB), yet it did not establish an explicit mathematical formulation for compensating model errors. Recent experimental results indicated that [16], in extremely close-range localization (30 mm), traditional sensor arrays exhibited a 27.6% increase in error due to magnetic field coupling effects, and existing denoising methods—such as wavelet basis function optimization—are inadequate to correct the inherent biases of the models, with the error magnitude being correlated to the magnet's shape, size, and material.

In view of these threefold limitations in existing methods (model-data discrepancies, limited generalization capability, and real-time bottlenecks), this study proposes a two-stage, physics-data fusion-based magnet localization calibration strategy. The main innovations include:

1) A physics-informed residual network is designed to correct systematic deviations in simulated data using dipole theory as a prior;
2) An interpolable lookup table optimization is employed, which utilizes distance-weighted trilinear interpolation combined with spherical linear interpolation (Slerp) to achieve sub-millimeter rapid matching.

Experimental results demonstrate the effectiveness of our approach. On a real-world test set, PIRNet significantly reduces the average positioning and orientation errors by over 45% and 68% respectively, compared to the baseline Levenberg-Marquardt (LM) algorithm applied to the uncorrected dipole model. Critically, this high performance is achieved with remarkable data efficiency, reducing the dependency on real-world training data by more than 90% compared to conventional data-driven methods. By integrating physical models with deep learning, our method offers a high-precision, low-cost, and robust solution for magnetic localization.

The remainder of the paper is structured as follows: In Section II, we introduce the mathematical model for single-magnet localization and the proposed optimization and neural network calibration methods, followed by the lookup table compensation method. Experimental results demonstrating the effectiveness of our approach are provided in Section III. Finally, Section IV concludes the paper and discusses future research directions.

II. Mathematical Model And Magnet Tracking Algorithm

A. Magnetic Dipole Model

When the size of the permanent magnet is much smaller than the distance from the permanent magnet to the target point, it can be regarded as a magnetic dipole. In the coordinate system in Fig. 1, the center of the magnet is represented by the position vector, and the sensor is placed at the position. The magnetic field components at a measurement

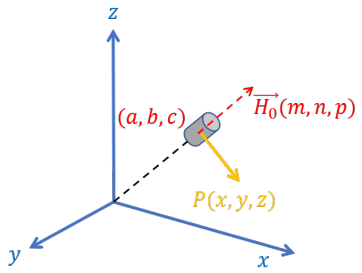

Fig. 1: Magnetic dipole model and coordinate system for magnet's localization. In the coordinate system, (x,y,z) is point P in space with coordinates, (m,n,p) is the direction of the magnetic moment with coordinates, and (a,b,c) is the position of the magnet.

point are given by and its magnetic field intensity is:

$$\mathbf{B}_i = B_{ix}\hat{\mathbf{i}} + B_{iy}\hat{\mathbf{j}} + B_{iz}\hat{\mathbf{k}} = B_T\left(\frac{3(\mathbf{H}\cdot\mathbf{P}_i)\mathbf{P}_i}{R_i^5} - \frac{\mathbf{H}}{R_i^3}\right) \quad (1)$$

where $i = 1,2,3,\ldots,N$, $B_T = \mu_r\mu_0 M_T/4\pi$. B_{ix}, B_{iy}, and B_{iz} are the three components in this position; N is the total number of sensors; μ_r is the relative magnetic permeability ($\mu_r \approx 1$ in air); μ_0 is the vacuum permeability, M_T is a constant characterizing the magnetic field strength of the magnet (related to the volume and magnetization). $\mathbf{P}_i$ is the vector of the position of the first sensor relative to the magnet center; R_i is the module of $\mathbf{P}_i$, that is:

$$R_i = \sqrt{(x_i-a)^2 + (y_i-b)^2 + (z_i-c)^2} \quad (2)$$

Magnetic dipole magnetic field vector $\mathbf{H} = [m,n,p]^T$ is and satisfies:

$$m^2 + n^2 + p^2 = 1 \quad (3)$$

The orthogonal components of $\mathbf{B}_i$ in three directions are:

$$B_{ix} = B_T\left[\frac{3[m(x_i-a)+n(y_i-b)+p(z_i-c)](x_i-a)}{R_i^5} - \frac{m}{R_i^3}\right] \quad (4)$$

$$B_{iy} = B_T\left[\frac{3[m(x_i-a)+n(y_i-b)+p(z_i-c)](y_i-b)}{R_i^5} - \frac{n}{R_i^3}\right] \quad (5)$$

$$B_{iz} = B_T\left[\frac{3[m(x_i-a)+n(y_i-b)+p(z_i-c)](z_i-c)}{R_i^5} - \frac{p}{R_i^3}\right] \quad (6)$$

$[a,b,c]$ and $[m,n,p]^T$ need to be solved using equations (3)–(6). There are 6 unknown parameters to be solved. We define the target error function as follows:

$$E = E_x + E_y + E_z \quad (7)$$

Combined with Equations (4) to (7), the error of each axis

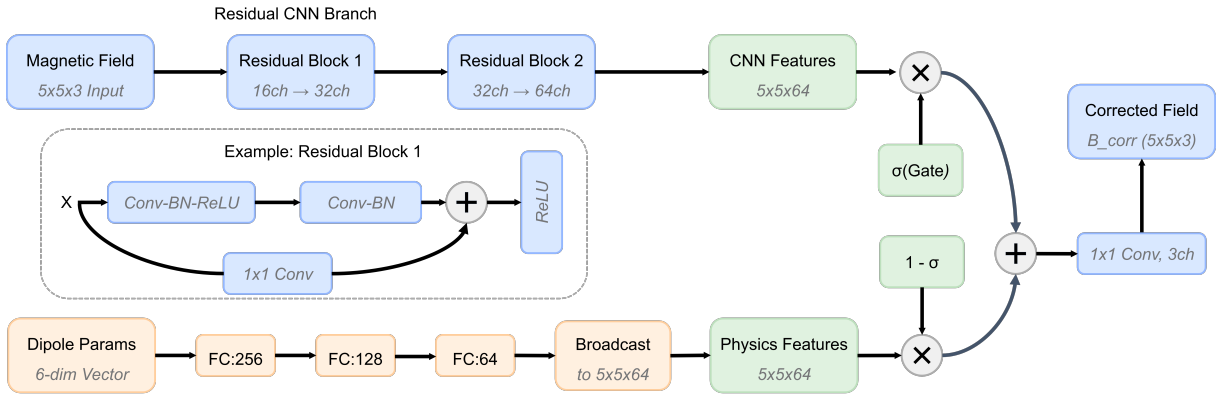

Fig. 2: Architecture of Physics-Informed Residual Network.

vector is obtained as follows:

$$E_x = \sum_{i=1}^{N} \left\{ B_{ix} - B_T \left[\frac{3[\ldots](x_i - a)}{R_i^5} - \frac{m}{R_i^3} \right] \right\}^2 \quad (8)$$

$$E_y = \sum_{i=1}^{N} \left\{ B_{iy} - B_T \left[\frac{3[\ldots](y_i - b)}{R_i^5} - \frac{n}{R_i^3} \right] \right\}^2 \quad (9)$$

$$E_z = \sum_{i=1}^{N} \left\{ B_{iz} - B_T \left[\frac{3[\ldots](z_i - c)}{R_i^5} - \frac{p}{R_i^3} \right] \right\}^2 \quad (10)$$

where $[\ldots]$ represents $[m(x_i-a)+n(y_i-b)+p(z_i-c)]$.

B. Physics-Informed Residual Network (PIRNet)

To address the discrepancy between the ideal dipole model and real-world sensor data, we propose a Physics-Informed Residual Network (PIRNet). The core idea is to learn a residual correction $\Delta\mathbf{B}$ such that the corrected field $\mathbf{B}_{\text{corr}} = \mathbf{B}_{\text{sim}} + \Delta\mathbf{B}$ accurately approximates the real field $\mathbf{B}_{\text{real}}$. As shown in Fig. 2, PIRNet features a dual-branch architecture.

1) **Dual-Branch Architecture:** The network processes two distinct inputs to model different error sources. A Residual CNN Branch, composed of several convolutional residual blocks, takes the simulated magnetic field $\mathbf{B}_{\text{sim}}$ as input to extract local, sensor-level distortion features, outputting $\mathbf{F}_{\text{cnn}}$. A Physics Encoder Branch, consisting of fully-connected layers, takes the 6-dim dipole parameters $\mathbf{p}$ as input to model systematic, pose-dependent deviations. Its output vector is then spatially broadcast to form a feature map $\mathbf{F}_{\text{phy}}$ of the same dimension as $\mathbf{F}_{\text{cnn}}$.
2) **Gated Fusion and Output:** The two feature maps are intelligently combined using a gated fusion mechanism, which dynamically weights $\mathbf{F}_{\text{cnn}}$ and $\mathbf{F}_{\text{phy}}$ before summation. The resulting fused features are then decoded by an output head (a 1x1 convolutional layer) to produce the final 5×5×3 residual correction $\Delta\mathbf{B}$.
3) **Physics-Informed Training:** Our key to achieving high accuracy with minimal real-world data lies in a two-phase training strategy. The network is first pre-trained on a large corpus of simulated data to learn the fundamental physics and model characteristics.

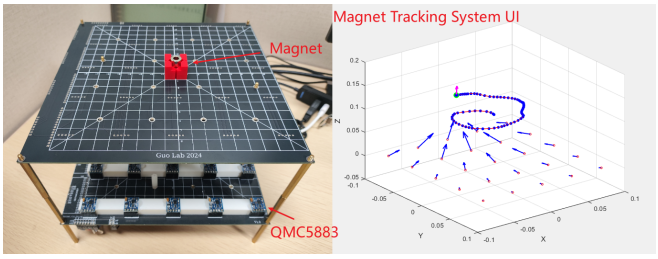

Fig. 3: Experimental platform comprising a magnetometer array (QMC5883), a scale plate, and an annular NdFeB magnet (grade: N45, outer radius $r_o = 10\,\text{mm}$, inner radius $r_i = 5\,\text{mm}$, and length $L = 10\,\text{mm}$). The direction and length of the blue arrow in the UI represents the direction and strength of the magnetic field detected by each sensor.

Subsequently, it is fine-tuned on a small, targeted real-world dataset to adapt to specific sensor noise and environmental interference. In both phases, a composite loss function is employed to guide the training:

$$L = (1-\lambda)\|(\mathbf{B}_{\text{sim}} + \Delta\mathbf{B}) - \mathbf{B}_{\text{real}}\|^2 + \lambda\|\nabla \cdot \Delta\mathbf{B}\|^2 \quad (11)$$

where $\mathbf{B}_{\text{real}}$ represents the corresponding ground-truth data for each phase. The second term enforces the divergence-free constraint ($\nabla \cdot \mathbf{B} = 0$), guiding the network to generate physically consistent corrections.

C. Levenberg-Marquardt (LM) Algorithm

The Levenberg-Marquardt (LM) algorithm is a widely used optimization technique for solving nonlinear least-squares problems. It combines the advantages of the Gauss-Newton method and gradient descent, offering robust performance even when initial parameter estimates are far from the true solution. This makes it particularly effective in applications like magnetic localization, where precise parameter estimation is crucial. In magnetic localization, we use equations (7) as the target function. LM algorithm iteratively adjusts the estimated position and orientation of a magnetic source to minimize the error between observed and predicted magnetic field measurements [10], [12], [15].

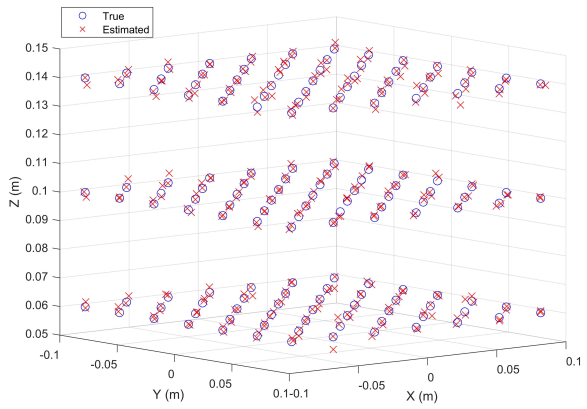

Fig. 4: 3D position distribution and results of Real-World datas of 147 samples at 60 to 140 mm height.

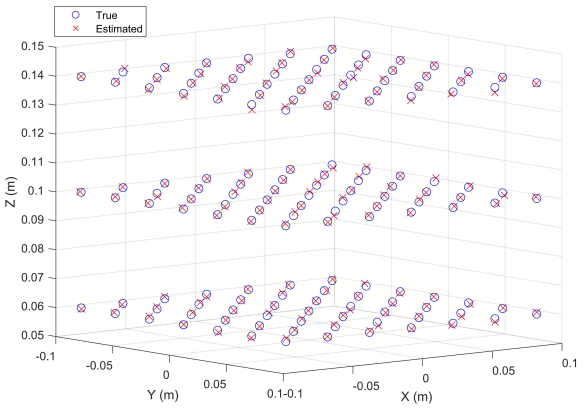

Fig. 6: 3D position distribution and results of the final corrected results of 147 samples at 60mm to 140mm height.

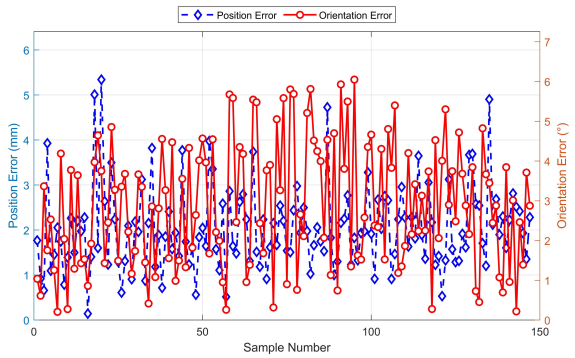

Fig. 5: Position errors and orientation errors of Real-World datas for 147 samples of the test set.

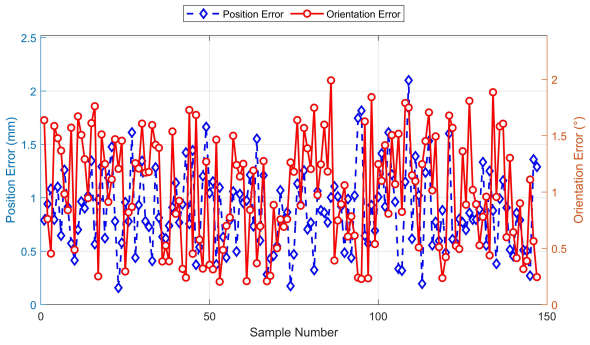

Fig. 7: Position errors and orientation errors of the final corrected results for 147 samples of the test set.

D. Lookup Table Compensation Method

To balance computational efficiency and physical consistency in magnetic localization, we propose a hybrid interpolation strategy combining linear interpolation for positional parameters and spherical linear interpolation (Slerp) for orientation parameters. For the corrected position $(\mathbf{a}_q, \mathbf{b}_q, \mathbf{c}_q)$, we perform trilinear interpolation over the 3D workspace grid (resolution: 20 mm). Given a query point $(\mathbf{a}_q, \mathbf{b}_q, \mathbf{c}_q)$, its interpolated value is calculated as:

$$\mathbf{B}_{\text{interp}} = \sum_{i=0}^{1}\sum_{j=0}^{1}\sum_{k=0}^{1} w_{(i,j,k)}\mathbf{B}(a_{i\Delta}, b_{j\Delta}, c_{k\Delta}) \tag{12}$$

where $w_{(i,j,k)}$ are normalized weights based on relative Euclidean distances between the query point and its 8 nearest neighbors in the lookup table.

For orientation parameters $(\mathbf{m}_1, \mathbf{n}_1, \mathbf{p}_1)$, we treat them as unit vectors on a 3D sphere and apply Slerp to maintain directional continuity:

$$\mathbf{m}_{\text{interp}} = \frac{\sin((1-t)\theta)}{\sin\theta}\mathbf{m}_1 + \frac{\sin(t\theta)}{\sin\theta}\mathbf{m}_2 \tag{13}$$

where $\theta = \cos^{-1}(\mathbf{m}_1 \cdot \mathbf{m}_2)$ is the angle between two orientation vectors, and $t \in [0,1]$ is the interpolation parameter.

III. Experimental Results

A. Magnetic Tracking System

In this study, as it shows in Fig. 3 a single annular NdFeB magnet was adopted as the magnetic target. As shown in Fig. 3, a self-developed magnetometer array consists of 25 tri-axis magnetometers (QMC5883, QST Corp.) evenly distributed on a 180×180 mm PCB board. A microcontroller unit (GD32F470ZGT6, GigaDevice) collected the magnetometer data and then transmitted it to a personal computer running Windows 11 with an Intel i7-12700 and a NVIDIA GeForce GTX 1660Ti. To obtain high-accuracy ground-truth data for error evaluation, the magnet's real-time pose was simultaneously recorded by a NOKOV Motion Capture System (Mars 2H), which provided sub-millimeter accuracy.

B. Datasets

Our dataset construction integrates model-driven simulation and real-world measurement to achieve robust few-shot learning, inspired by prior knowledge fusion approaches [11]. The dataset comprises two main components:

- **Prior Model-based Simulation Data:** We generated 58,320 simulated samples on a dense grid covering the workspace ([−80 mm, 80 mm] in x-y, [60 mm, 140 mm] in z). Each sample, computed via the magnetic dipole

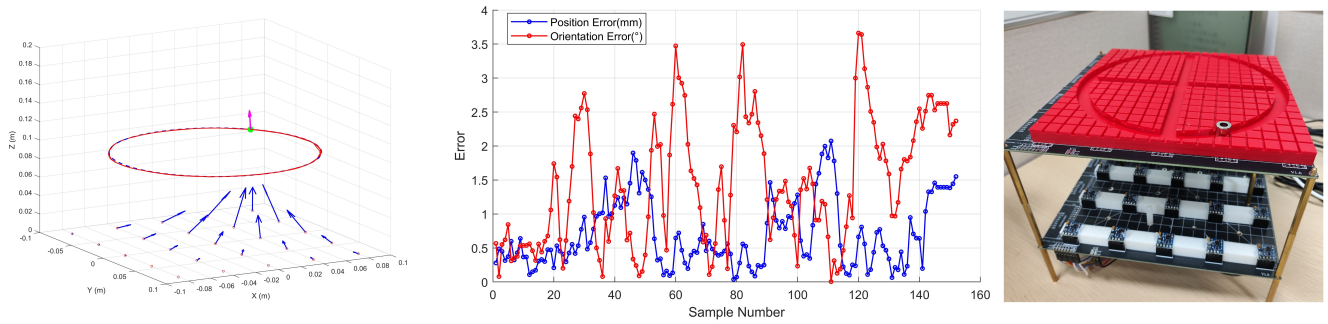

Fig. 8: Repeated accuracy testing. (a) Three-dimensional trajectory reconstruction of the magnet captured by the control software, with blue and red curves representing the actual manual displacement and real-time computational trajectory, respectively. (b) Tracking error of the magnet. (c) Experimental configuration for dynamic validation, featuring a magnet-constrained track system enabling manual trajectory execution.

model, was augmented with synthetic noise to simulate sensor imperfections.

- **Real-World Measurement Data:** A sparse set of 288 unique physical configurations was collected. For each configuration, 50 repeated measurements were acquired to capture intrinsic sensor noise, totaling 14,400 real-world samples.

The network is trained using a two-phase strategy: it is first pre-trained on the simulated dataset to learn the physical model's characteristics, and then fine-tuned on a small portion of the real-world data (11,520 training samples, 2,880 for validation) to adapt to real-world conditions. This hybrid approach significantly reduces the dependency on extensive real-world data collection. Compared to purely data-driven methods that often require thousands of unique samples to generalize, our method demonstrates high accuracy using only the 288 real-world configurations for adaptation. This represents a substantial improvement in data efficiency, calculated to be over 90%.

C. Static Magnet Positioning and Orientation Experiments

To evaluate the positioning accuracy, the positioning error E_p and the orientation error E_o are defined as:

$$\begin{cases} E_p = \sqrt{(a_e - a_t)^2 + (b_e - b_t)^2 + (c_e - c_t)^2} \\ E_o = \sqrt{(m_e - m_t)^2 + (n_e - n_t)^2 + (p_e - p_t)^2} \end{cases} \tag{14}$$

The orientation error can also be expressed in Euler angles, calculated by $2\sin^{-1}(E_o/2)$ [12].

The positioning performance of the Real-World data is shown in Figs. 4 and 5, where Fig. 5 shows the error analysis for Fig. 4. According to Figs. 4 and 5, the position error and orientation error will be relatively large without using the look-up table compensation method. The average error reached 2.1 mm and 3.23°. The positioning performance is shown in Figs. 6 and 7, where Fig. 7 shows the error analysis for Fig. 6. According to Figs. 6 and 7, through lookup table compensation method can successfully track the magnet with a high pose accuracy of 1.15 mm and 1.01°, in the distribution height from 60 to 140 mm.

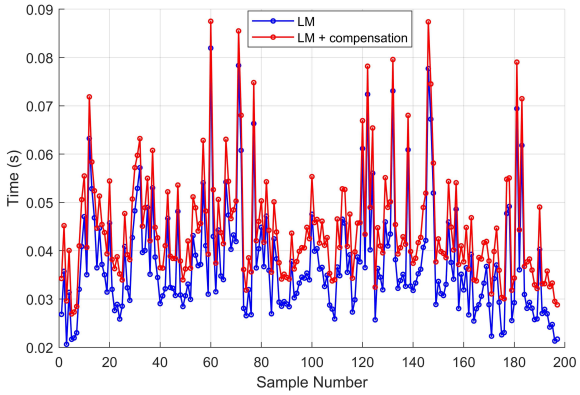

Fig. 9: Computation time.

D. Dynamic Magnet Tracking Experiment

To verify the tracking performance of the localization system, a dynamic experiment was carried out with a magnet. Fig. 8 shows a trace where the radius of the circle is 82.5 mm. The trajectory constraint of the magnet is carried out to verify the tracking effect of the positioning system on the magnet. The track is mounted on the experimental platform. Then, the magnet was manually moved slowly in the track, rotated 5 times, and the position of the magnet was recorded in real time. Fig. 8(b) shows the tracking error for one revolution of the magnet. The maximum tracking error is 2.07 mm and 3.6°. The average tracking error is 0.7 mm and 1.07°. In the dynamic experiments, the true trajectory is very similar to the estimated trajectory, which indicates that the positioning system has good tracking performance and can meet the tracking requirements. The reason for the large angle mutation error is that the magnet is hindered in moving in the guide rail, and the angle jitter occurs when the magnet is dragged.

E. Calculation Speed Experiment

The positioning system is used for position feedback, so the time required for positioning is also one of the important

indicators to evaluate the quality of positioning algorithm. In the speed experiment, the magnet moved randomly in the working interval, and used the LM algorithm and the linear compensation look-up table method to calculate the position and attitude of the magnet. In the process of magnet movement, the best quality obtained by the previous LM algorithm was used as the initial value of the next optimization algorithm to reduce the number of iterations and improve the optimization speed. In Fig. 9, we can see that the linear compensation table lookup method improves the computation time, but it is worth noting that the time improvement is not much: The average time of locating the magnet using LM algorithm alone is 37.4 ms (26.7 FPS), and the average time of locating the magnet using LM algorithm plus linear compensation table lookup method is 44.7 ms (22.4 FPS). In the process of magnet positioning, the increase of this time will not bring much influence.

F. Discussion

As demonstrated in Table I, the proposed PIRNet method exhibits a substantial improvement in accuracy compared to the baseline approach, which applies the Levenberg-Marquardt (LM) algorithm directly to the uncorrected dipole model. Specifically, by introducing the physics-informed residual correction, the mean positioning error was reduced by 45.2% (from 2.1 mm to 1.15 mm), and the orientation error was reduced by 68.7% (from 3.23° to 1.01°).

While the baseline LM algorithm shows a faster raw computation speed, our PIRNet-enhanced approach maintains a real-time performance of approximately 22.4 FPS, which is sufficient for most magnetic navigation applications. This slight trade-off in speed is overwhelmingly justified by the dramatic gain in accuracy and robustness. Crucially, this performance is achieved with high data efficiency (as discussed in Section III-B), highlighting our method's primary advantage over purely data-driven techniques. Future work will focus on model deployment optimization for embedded systems.

TABLE I: Performance Comparison With Baseline

Method	**Pos. Error (mm) [Mean]**	**Orient. Error (°) [Mean]**	**Speed (FPS)**
LM on Dipole Model (Baseline)	2.1	3.23	∼26.7
Ours	1.15	1.01	∼22.4

IV. Conclusion

This paper proposed a Physics-Informed Residual Network (PIRNet) based method for magnetic dipole model correction and high-precision localization. By integrating convolutional neural network feature extraction with magnetic dipole equation constraints, we successfully achieved robust sim-to-real transfer. Experimental results demonstrated that our approach reduced localization error from 2.1 mm to 1.15 mm and orientation error from 3.23° to 1.01°. Compared with the traditional LM algorithm and end-to-end deep learning solutions, the proposed method maintained real-time performance (22.4 FPS) while ensuring physical interpretability and environmental robustness, and it also collected much less real datasets than end-to-end deep learning. This research provided a high-precision, low-cost localization solution for magnetic navigation robots, showing significant application potential in minimally invasive surgical navigation and industrial inspection. In the future, we will develop embedded deployment solutions to enhance real-time performance.

References

[1] L. Zheng, S. Guo, and M. Kawanishi, "Multimodular Capsule Robot System With Drug Release for Intestinal Treatment," *IEEE Sensors Journal*, vol. 23, no. 16, pp. 18 568–18 578, Aug. 2023.

[2] Z. Wang, S. Guo, J. Guo, Q. Fu, L. Zheng, and T. Tamiya, "Selective Motion Control of a Novel Magnetic-Driven Minirobot With Targeted Drug Sustained-Release Function," *IEEE/ASME Transactions on Mechatronics*, vol. 27, no. 1, pp. 336–347, Feb. 2022.

[3] Y. Yan, S. Guo, B. Shen, C. Lyu, M. Ding, P. Yang, Y. Zhang, Y. Zhang, and J. Liu, "5-DOF microcoil positioning system utilizing single-axis electromagnetic transmitter," *IEEE/ASME Transactions on Mechatronics*, pp. 1–12, 2025.

[4] S. Liu and H. Wang, "A Wireless 6-DoF Pose Tracking System Using a Triaxially Anisotropic Soft Magnet," *IEEE/ASME Transactions on Mechatronics*, pp. 1–12, 2024.

[5] L. Zheng, S. Guo, and M. Kawanishi, "Magnetically Controlled Multifunctional Capsule Robot for Dual-Drug Delivery," *IEEE Systems Journal*, vol. 16, no. 4, pp. 6413–6424, Dec. 2022.

[6] L. Zheng, S. Guo, Z. Wang, and T. Tamiya, "A Multi-Functional Module-Based Capsule Robot," *IEEE Sensors Journal*, vol. 21, no. 10, pp. 12 057–12 067, May 2021.

[7] Y. Xu, K. Li, Z. Zhao, and M. Q.-H. Meng, "Adaptive Simultaneous Magnetic Actuation and Localization for WCE in a Tubular Environment," *IEEE Transactions on Robotics*, vol. 38, no. 5, pp. 2812–2826, Oct. 2022.

[8] Q. Shi, T. Liu, S. Song, J. Wang, and M. Q.-H. Meng, "An Optically Aided Magnetic Tracking Approach for Magnetically Actuated Capsule Robot," *IEEE Transactions on Instrumentation and Measurement*, vol. 70, pp. 1–9, 2021.

[9] K. Li, Y. Xu, Z. Zhao, and M. Q.-H. Meng, "External and internal sensor fusion based localization strategy for 6-DOF pose estimation of a magnetic capsule robot," *IEEE Robotics and Automation Letters*, vol. 7, no. 3, pp. 6878–6885, Jul. 2022.

[10] F. Masiero, V. Ianniciello, R. Raeli, E. Sinibaldi, L. Masia, and C. Cipriani, "Preliminary Assessment of Accurate Motion Detection via Magnetic Tracking towards Wearable Technologies," *IEEE Transactions on Medical Robotics and Bionics*, pp. 1–1, 2024.

[11] S. Su, S. Yuan, M. Xu, H. Gao, X. Yang, and H. Ren, "AMagPoseNet: Real-Time Six-DoF Magnet Pose Estimation by Dual-Domain Few-Shot Learning From Prior Model," *IEEE Transactions on Industrial Informatics*, vol. 19, no. 9, pp. 9722–9732, Sep. 2023.

[12] Q. Zhang, Y. Li, H. Xu, X. Li, and X. Zhang, "Magnetic Localization Method of Capsule Endoscope Based on Hybrid Model," *IEEE Transactions on Instrumentation and Measurement*, vol. 72, pp. 1–10, 2023.

[13] V. Schlageter, P.-A. Besse, R. Popovic, and P. Kucera, "Tracking system with five degrees of freedom using a 2D-array of Hall sensors and a permanent magnet," *Sensors and Actuators, A: Physical*, vol. 92, no. 1-3, pp. 37–42, Aug. 2001.

[14] S. Su, H. Dai, Y. Zhang, S. Yuan, S. Song, and H. Ren, "Magnetic Tracking With Real-Time Geomagnetic Vector Separation for Robotic Dockable Charging," *IEEE Transactions on Intelligent Transportation Systems*, vol. 24, no. 12, pp. 13 830–13 840, Dec. 2023.

[15] P. Guo, H. Dai, Q. Yang, Q. Huang, and H. Yao, "An Improved Magnetic Tracking Approach Based on ResNet-LM Fusion Algorithm," *IEEE Transactions on Instrumentation and Measurement*, vol. 71, pp. 1–10, 2022.

[16] H. Dai, C. Hu, S. Su, M. Lin, and S. Song, "Geomagnetic Compensation for the Rotating of Magnetometer Array During Magnetic Tracking," *IEEE Transactions on Instrumentation and Measurement*, vol. 68, no. 9, pp. 3379–3386, Sep. 2019.